

Sterile neutrinos with eV masses in cosmology – how disfavoured exactly?

Jan Hamann,^a Steen Hannestad,^a Georg G. Raffelt^b and Yvonne Y. Y. Wong^c

^aDepartment of Physics and Astronomy
University of Aarhus, DK-8000 Aarhus C, Denmark

^bMax-Planck-Institut für Physik (Werner-Heisenberg-Institut)
Föhringer Ring 6, D-80805 München, Germany

^cInstitut für Theoretische Teilchenphysik und Kosmologie
RWTH Aachen, D-52056 Aachen, Germany

E-mail: hamann@phys.au.dk, sth@phys.au.dk, raffelt@mppmu.mpg.de,
yvonne.wong@physik.rwth-aachen.de

Abstract. We study cosmological models that contain sterile neutrinos with eV-range masses as suggested by reactor and short-baseline oscillation data. We confront these models with both precision cosmological data (probing the CMB decoupling epoch) and light-element abundances (probing the BBN epoch). In the minimal Λ CDM model, such sterile neutrinos are strongly disfavoured by current data because they contribute too much hot dark matter. However, if the cosmological framework is extended to include also additional relativistic degrees of freedom beyond the three standard neutrinos and the putative sterile neutrinos, then the hot dark matter constraint on the sterile states is considerably relaxed. A further improvement is achieved by allowing a dark energy equation of state parameter $w < -1$. While BBN strongly disfavours extra radiation beyond the assumed eV-mass sterile neutrino, this constraint can be circumvented by a small ν_e degeneracy. Any model containing eV-mass sterile neutrinos implies also strong modifications of other cosmological parameters. Notably, the inferred cold dark matter density can shift up by 20–75% relative to the standard Λ CDM value.

Contents

1	Introduction	1
2	CMB and LSS	2
2.1	Cosmological data	2
2.2	Cosmological models	3
2.3	Goodness-of-fit	3
2.4	Effects on other cosmological parameters	4
3	Big bang nucleosynthesis	5
3.1	Analysis	5
3.2	Uncertainties of input data	6
3.3	Primordial element abundance data and likelihood functions	7
3.4	BBN with sterile neutrinos	8
3.5	Degenerate BBN with sterile neutrinos	8
3.6	Combining BBN with CMB+LSS data	11
4	Conclusions	11

1 Introduction

There is mounting evidence from reactor and short-baseline neutrino oscillation experiments suggesting the existence of one or two sterile neutrinos with mass splittings relative to the active flavours in the neighbourhood of $\Delta m^2 \sim 1 \text{ eV}^2$ and fairly large mixing parameters (see, e.g., [1] for a review and global interpretation, and [2–4] for other recent analyses). In the early universe, flavour oscillations would bring these sterile states into thermal equilibrium prior to neutrino decoupling at $T \sim 1 \text{ MeV}$, thereby increasing the relativistic energy density (see, e.g., [5] for a review). This increase, commonly parameterised in terms of an additional contribution to the relativistic neutrino degrees of freedom N_{eff} , significantly modifies big-bang nucleosynthesis (BBN) of light elements, the cosmic microwave background (CMB) anisotropies, and the formation of large-scale structures (LSS). By the same token, these eV-mass sterile neutrinos would later play the role of a non-negligible hot-dark matter component.

The cosmological verdict on eV-mass sterile neutrinos is somewhat mixed. Current CMB and LSS observations show a consistent preference for additional relativistic degrees of freedom beyond the standard model expectation of $N_{\text{eff}} = 3.046$, with low to moderate statistical significance [6–11]. On the other hand, if this putative radiation excess is interpreted in terms of sterile neutrinos, the usual hot dark matter limits constrain the sterile masses to the sub-eV regime. For example, in a 3+1 scenario consisting of three essentially massless active flavours and one fully thermalised sterile flavour, the sterile mass is constrained to $m_s \lesssim 0.5 \text{ eV}$ [7]. Thus, cosmology appears to disfavour the existence of one or two sterile states that have mass and mixing parameters favoured by a global analysis of the laboratory data.

However, both the tentative evidence for extra radiation and these hot-dark matter bounds are based on the simplest ΛCDM framework; extended models may provide different

answers. For example, if the dark energy equation of state parameter w and curvature Ω_k are used as fit parameters, the presence of eV-mass sterile neutrinos favours a w value much smaller than -1 [12]. Here, we take the view that it may be more natural to look for extensions to Λ CDM within the neutrino sector alone, for example in terms of additional radiation. (However, we note in passing that in certain dynamical dark energy models such as the mass varying neutrino scenario, a strongly modified neutrino sector is responsible for driving the dark energy evolution. In this sense, changing w may not be an entirely unnatural solution to the massive sterile neutrino problem.) Multiple sterile right-handed states may exist and some of them may even be lighter than the eV range. Moreover, the existence of sterile neutrinos also provides a means for the generation of large neutrino chemical potentials [13], which may be exploited to circumvent standard BBN bounds on the number of relativistic degrees of freedom.

The premise of our work is that sterile neutrino states with eV-range masses are real and that they are fully thermalised prior to neutrino decoupling. In addition, we allow for radiation beyond that due to the three standard flavours (assumed to be effectively massless) and beyond the eV-mass sterile neutrinos. We consider both data from precision cosmology and the constraints on N_{eff} imposed by BBN.

More specifically, in section 2 we investigate the impact of eV-mass sterile neutrinos on the inference of cosmological parameters from CMB and LSS observations. In section 3 we evaluate the constraints on additional relativistic species during the BBN epoch, using measurements of the primordial abundances of several light elements. In section 4 we summarise and discuss our results.

2 CMB and LSS

2.1 Cosmological data

The CMB anisotropies and the LSS distribution are sensitive to both additional relativistic degrees of freedom and the mass scale of light, free-streaming particles. To explore the impact of eV-mass sterile neutrinos on precision cosmology, we use CMB anisotropy data and their accompanying likelihood routines from the WMAP 7-year data release [14], as well as the ACBAR [15], BICEP [16], and QuAD [17] experiments. In addition, we use the halo power spectrum extracted from the SDSS-DR7 luminous red galaxy sample [18], and type Ia supernova (SN) data from the Union-2 compilation [19]. Finally, we impose a constraint on the Hubble parameter based on the Hubble Space Telescope observations [20]. We refrain from using observational data pertaining to very small length scales, such as estimates of small-scale density fluctuation amplitudes from the Lyman- α forest and cluster abundance. While these measurements are in principle an extremely powerful tool for constraining neutrino masses, they are also currently dominated by systematic uncertainties. We have tested explicitly that adding data from the Atacama Cosmology Telescope (ACT) [21] does not alter our results; The main role of ACT is to break parameter degeneracies in CMB-only analyses. These degeneracies are however already broken by the addition of LSS data.

We construct allowed regions in cosmological parameter space using standard Bayesian inference techniques. All posterior probability density functions are sampled using the Markov Chain Monte Carlo (MCMC) code `CosmoMC` [22].

Table 1. Definitions of the model parameters and the prior ranges imposed on them in our CMB+LSS likelihood analysis. Uniform priors are used for all listed parameters.

Parameter	Symbol	Prior
Baryon density	ω_b	$0.005 \rightarrow 0.1$
Cold dark matter density	ω_{cdm}	$0.01 \rightarrow 0.99$
Hubble parameter	h	$0.4 \rightarrow 1.0$
Amplitude of scalar spectrum @ $k = 0.05 \text{ Mpc}^{-1}$	$\log[10^{10} A_s]$	$2.7 \rightarrow 4$
Scalar spectral index	n_s	$0.5 \rightarrow 1.5$
Optical depth to reionisation	τ	$0.01 \rightarrow 0.8$
Number of extra massless neutrino degrees of freedom	ΔN_{ml}	$0 \rightarrow 5$
Dark energy equation of state parameter	w	$-2.5 \rightarrow -0.5$

2.2 Cosmological models

We consider three basic cosmological frameworks in which we embed light sterile neutrinos and analyse their consequences.

1. The Λ CDM class of models is defined by a flat spatial geometry and six free parameters, $\{\omega_b, \omega_{\text{cdm}}, h, A_s, n_s, \tau\}$. See table 1 for their definitions and prior ranges. Within this framework, we consider four possibilities in the neutrino sector: (a) 3 massless neutrinos (standard Λ CDM), (b) 3 massless+1 sterile (0 eV), (c) 3 massless+1 sterile (1 eV), and (d) 3 massless+1 sterile (2 eV).
2. In the second class of models, which we dub Λ CDM+ ΔN , we include additional relativistic degrees of freedom beyond the 3+1 standard and sterile neutrinos. We consider three scenarios: (a) 3+ ΔN_{ml} massless+1 sterile (0 eV), (b) 3+ ΔN_{ml} massless+1 sterile (1 eV), and (c) 3+ ΔN_{ml} massless+1 sterile (2 eV). Such models are especially sensitive to BBN constraints to be discussed in section 3.
3. The w CDM+ ΔN framework is a variant of Λ CDM+ ΔN , in which we extend the dark energy sector to include the possibility that $w \neq -1$.

2.3 Goodness-of-fit

We consider first the goodness-of-fit, as quantified by the best-fit effective χ^2 , of the cosmological models described in the previous section. Here the effective χ^2 is defined as $\chi_{\text{eff}}^2 = -2 \ln \mathcal{L}_{\text{max}}$, where \mathcal{L}_{max} is the maximum likelihood of the data given the model. Table 2 summarises the best-fit χ_{eff}^2 for these models and, where appropriate, the preferred values of ΔN_{ml} and w , using the data sets described in section 2.1. Some comments are in order.

1. Within the Λ CDM framework, a scenario with 3 massless neutrinos plus one fully thermalised massless sterile species offers a slightly better fit than standard Λ CDM ($\Delta\chi_{\text{eff}}^2 = -3.16$). However, once the sterile states have mass, the quality of the fit deteriorates. The 1 eV scenario is already marginally worse than standard Λ CDM by $\Delta\chi_{\text{eff}}^2 = 4.20$. The 2 eV model may be deemed unacceptable ($\Delta\chi_{\text{eff}}^2 = 21.41$).
2. The situation improves when we allow for additional radiation (Λ CDM+ ΔN). For example, if the sterile neutrino has a mass of 1 eV, the best-fit χ_{eff}^2 is comparable to

that of standard Λ CDM, albeit at the cost of admitting $\Delta N_{\text{ml}} \sim 1.5$ additional massless degrees of freedom. For a 2 eV sterile mass, we find $\Delta N_{\text{ml}} \sim 2.6$ and $\chi_{\text{eff}}^2 = 12.8$. This last result can be compared with the w CDM+ Ω_k model of reference [12], for which $\Delta\chi_{\text{eff}}^2 = 12$ assuming a *lighter* 1.33 eV sterile neutrino. Therefore, introducing extra radiation appears to be somewhat superior to modifying the dark energy sector at resolving the sterile mass conundrum.

3. Even more improvement is available if, in addition, we allow the dark energy equation of state parameter w to differ from -1 (w CDM+ ΔN). In this class of models, we see that a scenario with one species of 1 eV sterile neutrinos in fact provides a better fit to the data than does standard Λ CDM, with $\Delta\chi_{\text{eff}}^2 = -0.78$, at the expense of two additional free parameters.

Table 2. Best-fit $\Delta\chi_{\text{eff}}^2$ relative to the standard Λ CDM framework for the models described in section 2.2, using the data sets of section 2.1. We also show the best-fit values and 95%-credible upper and lower limits on ω_{cdm} , and, where appropriate, on ΔN_{ml} and w .

Framework	Neutrino sector	$\Delta\chi_{\text{eff}}^2$	ΔN_{ml}	w	ω_{cdm}
Λ CDM	3 massless	0	—	—	$0.1132^{+0.0036}_{-0.0082}$
	3 massless + 1 sterile (0 eV)	-3.16	—	—	$0.1299^{+0.0069}_{-0.0066}$
	3 massless + 1 sterile (1 eV)	4.20	—	—	$0.1398^{+0.0061}_{-0.0074}$
	3 massless + 1 sterile (2 eV)	21.41	—	—	$0.1473^{+0.0075}_{-0.0064}$
Λ CDM+ ΔN	3+ ΔN_{ml} massless + 1 sterile (0 eV)	-3.54	$0.01^{+1.12}_{-0.01}$	—	$0.133^{+0.023}_{-0.005}$
	3+ ΔN_{ml} massless + 1 sterile (1 eV)	2.26	$1.49^{+1.11}_{-0.73}$	—	$0.166^{+0.026}_{-0.017}$
	3+ ΔN_{ml} massless + 1 sterile (2 eV)	12.82	$2.57^{+1.24}_{-0.59}$	—	$0.192^{+0.031}_{-0.015}$
	3+ ΔN_{ml} massless + 1 sterile (2 eV)	7.80	$2.48^{+1.71}_{-0.79}$	—	$0.198^{+0.032}_{-0.019}$
w CDM+ ΔN	3+ ΔN_{ml} massless + 1 sterile (0 eV)	-5.38	$0.09^{+1.61}_{-0.09}$	$-1.00^{+0.18}_{-0.12}$	$0.132^{+0.032}_{-0.006}$
	3+ ΔN_{ml} massless + 1 sterile (1 eV)	-0.78	$1.23^{+1.61}_{-0.75}$	$-1.11^{+0.18}_{-0.21}$	$0.164^{+0.035}_{-0.015}$
	3+ ΔN_{ml} massless + 1 sterile (2 eV)	7.80	$2.48^{+1.71}_{-0.79}$	$-1.17^{+0.23}_{-0.22}$	$0.198^{+0.032}_{-0.019}$
	3+ ΔN_{ml} massless + 1 sterile (2 eV)	7.80	$2.48^{+1.71}_{-0.79}$	$-1.17^{+0.23}_{-0.22}$	$0.198^{+0.032}_{-0.019}$

2.4 Effects on other cosmological parameters

We have seen that precision cosmological observations can reasonably accommodate one fully thermalised species of massive sterile neutrinos if we allow also for additional massless degrees of freedom and/or a non-standard dark energy equation of state. An interesting consequence is that the preferred values of other free parameters of the model also shift accordingly.

The most notable example in this regard is the cold dark matter density ω_{cdm} . Figure 1 illustrates the shift in ω_{cdm} as a function of the sterile neutrino mass within the Λ CDM+ ΔN framework. Figure 2 is similar, but for the w CDM+ ΔN models. See also table 2 for the best-fit values and credible regions. Clearly, the larger the sterile neutrino mass, the larger the preferred value of ω_{cdm} . In the case of a 2 eV sterile neutrino, the upward shift in ω_{cdm} can be as large as 75% in the w CDM+ ΔN model, relative to the standard Λ CDM inferred value. This shift in the cold dark matter density can have importance consequences for, e.g., the SUSY dark matter parameter space.

Another affected parameter is the scalar spectral index n_s , whose preferred region widens in the presence of additional light species, as was also seen in our previous analysis [7].

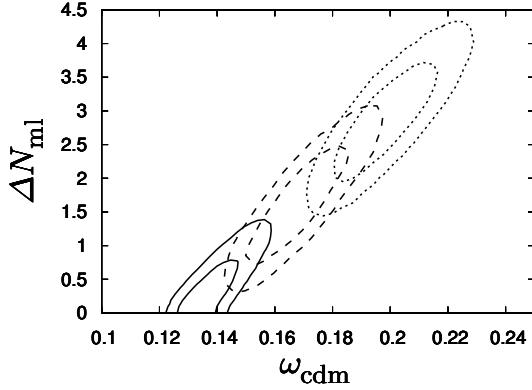


Figure 1. 2D marginal 68%- and 95%-credible regions in the $(\Delta N_{\text{ml}}, \omega_{\text{cdm}})$ -plane for three $\Lambda\text{CDM}+\Delta N$ class models containing one thermalised sterile species of mass $m_s = 0$ eV (solid), 1 eV (dashed), and 2 eV (dotted).

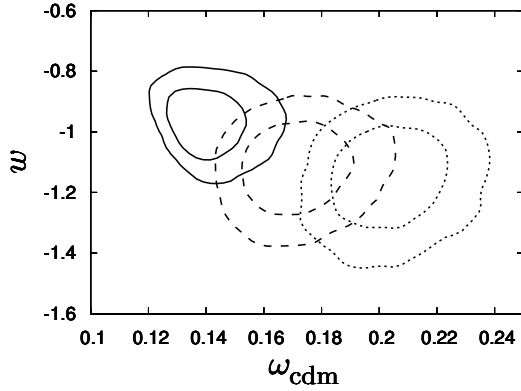


Figure 2. 2D marginal 68%- and 95%-credible regions in the (w, ω_{cdm}) -plane for three $w\text{CDM}+\Delta N$ class models containing one thermalised sterile species of mass $m_s = 0$ eV (solid), 1 eV (dashed), and 2 eV (dotted).

3 Big bang nucleosynthesis

While not sensitive to the masses of neutrinos, BBN has long been used to probe the radiation content of the Universe at temperatures of order 1 MeV [23–25]. In this section, we explore the implications of the latest primordial element abundance measurements on the sterile neutrino scenario. We consider a general BBN model with three free parameters: the baryon density ω_b , an extra N_s effective sterile neutrino species on top of the usual three fully thermalised standard neutrinos, and, eventually we also allow for the presence of a neutrino chemical potential ξ . Table 3 summarises the prior ranges for these parameters.

3.1 Analysis

We infer constraints on the BBN parameters with a modified version of the Markov Chain Monte Carlo (MCMC) sampler *CosmoMC* [22].¹ The *ParthENoPE* [26] code is employed to pre-calculate the primordial element abundances on a grid of points in (ω_b, N_s, ξ) -space. For each

¹The numerical module for implementing the BBN likelihood in *CosmoMC* is available from the corresponding author (Jan Hamann) upon request.

Table 3. Definitions of the model parameters and the prior ranges imposed on them in our BBN likelihood analysis. Uniform priors are used for all listed parameters.

Parameter	Symbol	Prior
Baryon density	ω_b	$0.01 \rightarrow 0.035$
Number of sterile neutrinos	N_s	$0 \rightarrow 5$
Neutrino chemical potential	ξ	$-0.2 \rightarrow 0.3$

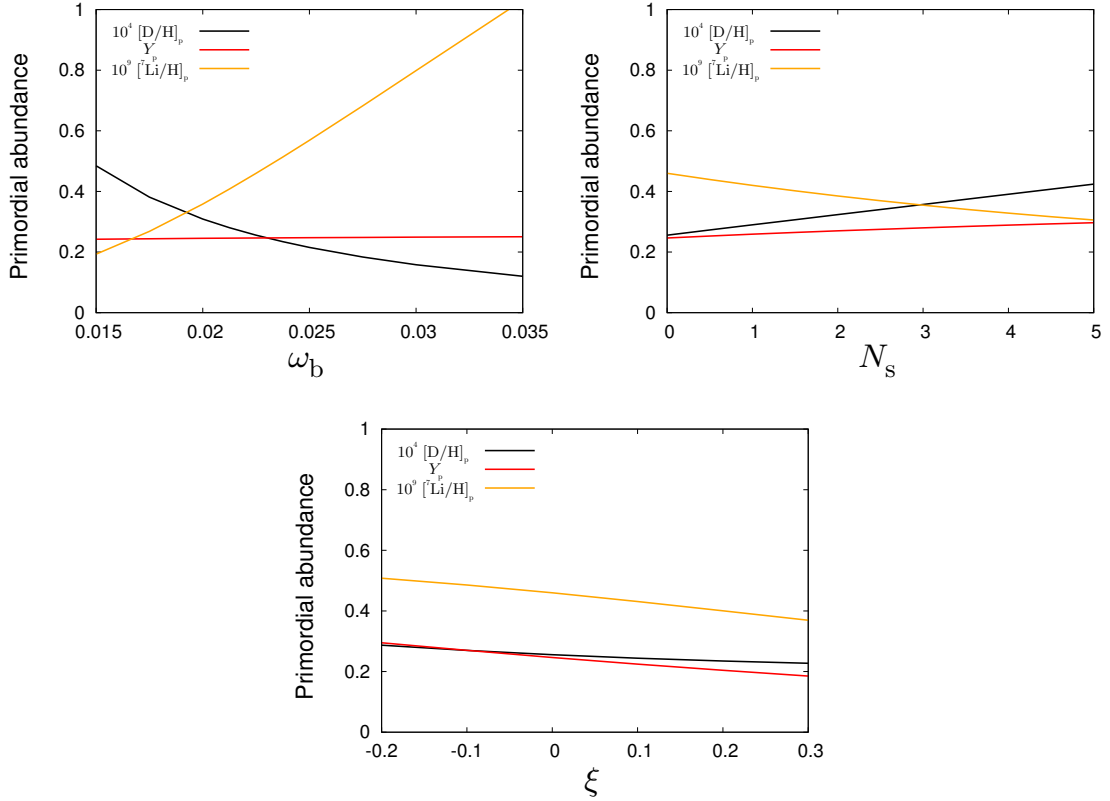


Figure 3. Primordial abundances of D, ${}^4\text{He}$ and ${}^7\text{Li}$ as functions of the cosmological parameters. *Top left:* dependence on ω_b for $N_s = \xi = 0$. *Top right:* dependence on N_s for $\omega_b = 0.0225$ and $\xi = 0$. *Bottom:* dependence on ξ for $\omega_b = 0.0225$ and $N_s = 0$.

set of parameter values the abundances are then obtained from the grid by 3-dimensional cubic spline interpolation. We illustrate the dependence of the light element abundances on the cosmological parameters on selected slices through parameter space in figure 3.

3.2 Uncertainties of input data

The output of **ParthENoPE** is subject to theoretical uncertainties from two principal sources: the nuclear reaction rates and the free neutron lifetime τ_n . The former induce a $\pm 1.6\%$ error for the D prediction, negligible error for ${}^4\text{He}$, and $\pm 8\%$ for ${}^7\text{Li}$ [27]. We fold these uncertainties into our definitions of the corresponding likelihood functions in section 3.3.

The main source of uncertainty for the predicted ${}^4\text{He}$ abundance is the free neutron lifetime. The Particle Data Group recommends a value of $\tau_n^{\text{PDG}} = 885.7 \pm 0.8$ s [28]. This,

however, appears to be in strong tension with recent measurements performed by Serebrov *et al.* [29], who found $\tau_n^S = 878.5 \pm 0.8$ s, and Pichlmair *et al.* [30], who measured $\tau_n^P = 880.7 \pm 1.8$ s. Although a re-analysis of neutron lifetime data shows that previous estimates may have been biased by $\sim +6$ s [31], we will nonetheless consider the two extreme values τ_n^S and τ_n^{PDG} in the following, in order to illustrate the possible impact of this uncertainty on our inference. Going from τ_n^S to τ_n^{PDG} shifts the Y_p prediction by $\sim 0.6\%$, whereas $[^2\text{D}/\text{H}]_p$ and $[^7\text{Li}/\text{H}]_p$ change by $\sim 0.3\%$ which is negligible compared with the effects of other uncertainties (nuclear rates and astrophysical measurements).

3.3 Primordial element abundance data and likelihood functions

Deuterium

The primordial deuterium abundance $[\text{D}/\text{H}]_p$ can be inferred from measurements of the absorption of quasar light in high-redshift low-metallicity hydrogen clouds. Pettini *et al.* [32] derive a value of $\log [\text{D}/\text{H}]_p = -4.55 \pm 0.03$ from the observation of the spectra of seven quasars. Taking into account the theoretical uncertainty of 1.6%, the corresponding likelihood function is

$$-2 \ln \mathcal{L}_D = \frac{\left(\log [\text{D}/\text{H}]_p + 4.55\right)^2}{0.034^2}. \quad (3.1)$$

Helium-4

The mass fraction Y of ^4He is determined by measuring helium and hydrogen emission lines in low-metallicity HII regions of dwarf galaxies. Its primordial value Y_p can then be estimated by treating Y as a function of metallicity Z and extrapolating to $Z = 0$. A linear regression of data from seven high-quality objects with a careful treatment of systematic uncertainties yields $Y_p = 0.2573^{+0.0033}_{-0.0088}$, with the additional restriction to theoretically meaningful positive slopes $dY/dZ > 0$ [33].² We therefore model the likelihood function as

$$-2 \ln \mathcal{L}_{^4\text{He}} = \begin{cases} \frac{(Y_p - 0.2573)^2}{0.0033^2}, & \text{if } Y_p \geq 0.2573, \\ \frac{(Y_p - 0.2573)^2}{0.0088^2}, & \text{if } Y_p < 0.2573. \end{cases} \quad (3.2)$$

Lithium-7

Lithium abundances have been determined from the spectra of metal-poor dwarf stars. At low metallicities, the lithium abundance appears to be independent of metallicity [37]. However, the measurements are subject to significant systematic uncertainties about the stars' temperatures. Additionally, the measured plateau value may not be representative of the primordial abundance: ^7Li can be generated by cosmic rays, or depleted through Population III stars or diffusion processes within the dwarf stars [38].

The Particle Data Group estimates an average of $[^7\text{Li}/\text{H}]_p = (1.7 \pm 0.06 \pm 0.44) \times 10^{-10}$, which is significantly lower than the standard BBN expectation for realistic baryon densities – the well-known lithium problem [39]. Approximating the 8% theoretical uncertainty with

²It has been argued that a linear regression may not necessarily be realistic in view of certain models of early ^4He production by Pop III stars [34], as for instance suggested in references [35, 36]. However, even in these cases, the difference between the primordial and the observed values of Y will not exceed ~ 0.01 , a possibility that is well covered by the lower limit on Y_p in equation (3.2).

an absolute error of $\sigma_{7\text{Li}}^{\text{nucl}} \simeq 0.4 \times 10^{-10}$ and adding the errors in quadrature, we arrive at the following likelihood function for lithium:

$$-2 \ln \mathcal{L}_{7\text{Li}} = \frac{(10^{10} [7\text{Li}/\text{H}]_{\text{p}} - 1.7)^2}{0.598^2}, \quad (3.3)$$

which will be considered only where appropriate.

CMB+LSS prior on the baryon density

In addition to primordial abundance measurements, we also consider a prior on the baryon density ω_{b} from CMB+LSS data as an independent constraint. Since the bounds on ω_{b} are in principle model-dependent, using results from a fit to the standard ΛCDM model as a prior for extended models would be technically incorrect. Instead we use the baryon density inferred within the $\Lambda\text{CDM}+N_{\text{s}}$ model, $\omega_{\text{b}} = 0.02255 \pm 0.00049$, to define our prior

$$-2 \ln \pi_{\text{CMB+LSS}}(\omega_{\text{b}}) \propto \frac{(\omega_{\text{b}} - 0.02255)^2}{0.00049^2}. \quad (3.4)$$

In practice, however, present CMB+LSS data are sufficiently sensitive to break any potential degeneracy between N_{s} and ω_{b} , so that the constraints on ω_{b} show no appreciable variation with respect to the inclusion or otherwise of the parameter N_{s} .

3.4 BBN with sterile neutrinos

We first consider a BBN scenario with N_{s} effective sterile neutrino species. The additional radiation energy density contributed by the sterile neutrinos increases the expansion rate at BBN, leading to a higher freeze-out temperature T_{f} . As a consequence, the equilibrium neutron-to-proton ratio $n/p = \exp(-\Delta m/T)$, where Δm is the neutron-proton mass difference, is larger at neutron freeze-out. The resulting Y_{p} is larger because almost all neutrons end up in ${}^4\text{He}$. Similarly, a larger neutron lifetime also increases the expected Y_{p} .

We show the constraints on the $(\omega_{\text{b}}, N_{\text{s}})$ parameter space from our analysis in figure 4. The top two panels illustrate the well-known fact that the deuterium abundance constrains mainly the baryon density, whereas constraints on N_{s} are mostly driven by the helium data. However, once we impose the CMB+LSS prior on ω_{b} , even the deuterium data alone significantly constrain N_{s} . This constraint is of interest in view of the helium data already being systematics-limited.

For a combined fit of the deuterium and the helium data, the best-fit value of N_{s} is 0.86, with a 95%-credible upper limit of $N_{\text{s}} < 1.26$ (or 1.24 if the CMB+LSS prior on ω_{b} is included). Using the larger neutron lifetime $\tau_{\text{n}}^{\text{PDG}}$, we obtain slightly lower values: a best-fit of 0.73 and a 95% upper limit of $N_{\text{s}} < 1.14$. The one-dimensional marginalised posterior probability densities for N_{s} are shown in figure 5. As already emphasised in reference [34], there is no strong indication for $N_{\text{s}} > 0$ from BBN alone – $N_{\text{s}} = 0$ lies well within the 90%-credible interval in all cases – owing to the relatively weak lower limit on Y_{p} . While one fully thermalised sterile neutrino species is slightly favoured over $N_{\text{s}} = 0$, two fully thermalised sterile neutrino species are clearly incompatible with the data in this scenario.

3.5 Degenerate BBN with sterile neutrinos

If we imagine for a moment that there were two sterile neutrino species today, how could this be reconciled with the results of the previous section? One possibility would be incomplete

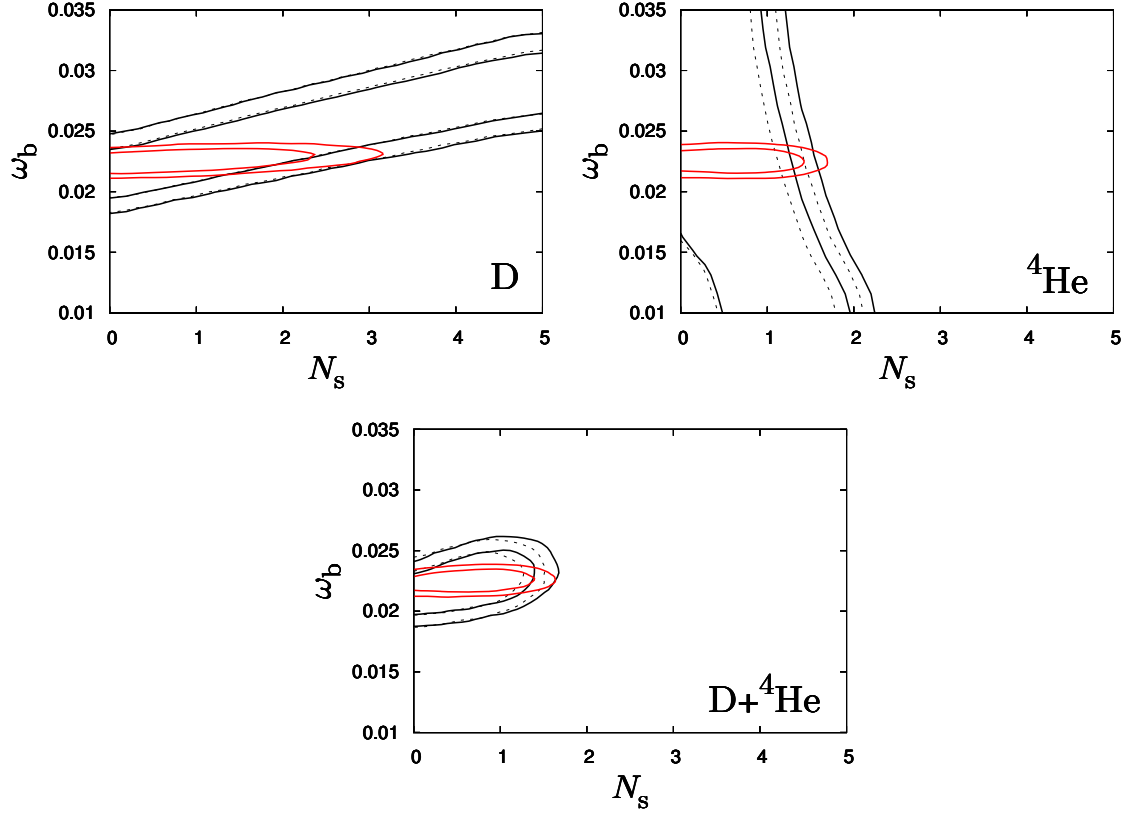


Figure 4. 2D marginal 90%- and 99%-credible regions in the (ω_b, N_s) -plane, assuming the BBN+sterile scenario. Black lines denote results from elemental abundance measurements alone (solid lines assume $\tau_n = 878.5$ s, dotted lines 885.7 s). The red lines include a CMB+LSS prior on ω_b . *Top left:* D data. *Top right:* ^4He data. *Bottom:* D+ ^4He data.

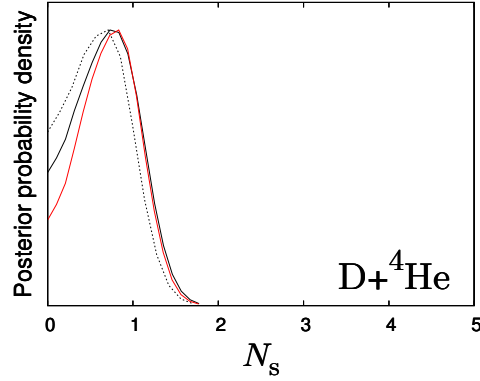


Figure 5. 1D posterior pdf for N_s , marginalised over ω_b , for the BBN+sterile scenario and D+ ^4He data. Same colour/line coding as in figure 4.

thermalisation, such that the effective N_s is smaller than 2; this scenario could be confirmed if future CMB+LSS data should find $N_{\text{eff}} < 5$. Alternatively, the sterile neutrinos could be the decay products of a heavy particle species between BBN and decoupling. In this case,

N_s could be smaller than 2 at BBN, but equal to or larger than 2 at decoupling.

A third possibility is the degenerate BBN scenario [40], in which all standard neutrinos share a common non-zero chemical potential ξ [41–43]. The presence of a chemical potential affects BBN in two ways. Firstly, it contributes an additional term to the effective radiation density,

$$\Delta N_{\text{eff}} = \frac{45}{7} \left[2 (\xi/\pi)^2 + (\xi/\pi)^4 \right]. \quad (3.5)$$

Secondly, the degeneracy in the electron neutrinos modifies the equilibrium neutron-to-proton ratio,

$$n/p = \exp \left(-\frac{\Delta m}{T} - \xi \right). \quad (3.6)$$

For $\xi \simeq \mathcal{O}(0.1)$, it is the latter effect that is most relevant for the resulting element abundances: a positive ξ will reduce the number of available neutrons with respect to the $\xi = 0$ case and thus suppress Y_p . This suppression can be used to circumvent the upper bound on N_s found in the previous section.

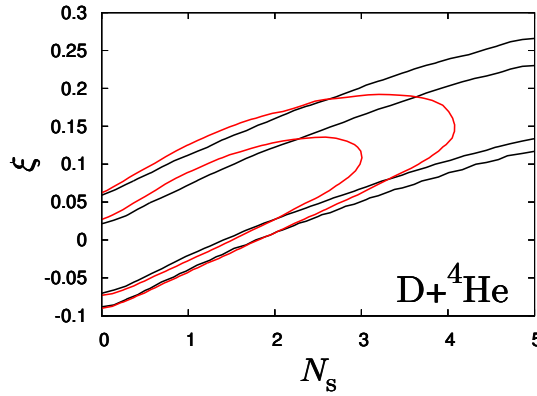


Figure 6. 2D marginal 90%- and 99%-credible regions in the (ξ, N_s) -plane marginalised over ω_b , assuming the degenerate BBN+sterile scenario and $\tau_n = 878.5$ s. The black lines denote results from $D+{}^4\text{He}$ data, while the red lines also include a CMB+LSS prior on ω_b .

Figure 6 shows the preferred region in the (ξ, N_s) -plane in the degenerate BBN scenario. In the 3-dimensional parameter space (ω_b, N_s, ξ) , the deuterium and the helium data can only constrain two directions, leaving an unconstrained one which admits arbitrarily high values of N_s . Only by adding the CMB+LSS prior on ω_b are we able to obtain any constraint at all: we find a best-fit of $N_s = 0.79$ and a 95%-credible upper limit of $N_s < 2.56$. Conversely, if we assume $N_s = 2$, a positive non-zero chemical potential is required: $0.03 < \xi < 0.14$ (95%-credible interval), with a best-fit value of $\xi = 0.064$.

As can be seen from figure 3, larger values of N_s and ξ both lead to a lower prediction for the primordial ${}^7\text{Li}$ abundance. Taking for instance $N_s = 2$, $\xi = 0.066$ and $\omega_b = 0.0225$, one obtains $[{}^7\text{Li}/\text{H}]_p = 0.372 \times 10^{-10}$ (compared to $[{}^7\text{Li}/\text{H}]_p = 0.460 \times 10^{-10}$ for $N_s = \xi = 0$). While this is still 3.4 standard deviations larger than the measured value, the discrepancy is not quite as serious as the 4.8 standard deviations one finds in standard BBN.

3.6 Combining BBN with CMB+LSS data

If one assumes that neither ω_b nor N_{eff} changed between the BBN era and the time of photon decoupling, one could perform a combined analysis of the CMB+LSS and BBN data in analogy to the previous literature [44, 45].

With the stringent upper bound on the radiation density from the standard BBN setting, it is clear that the scenarios with one eV-mass sterile neutrino plus extra massless degrees of freedom considered in section 2 will fit the combined data rather badly: for a 1 eV (2 eV) sterile neutrino, the $\Lambda\text{CDM}+\Delta N$ model yields $\Delta\chi_{\text{eff}}^2 \simeq 9$ (19), relative to ΛCDM . This, in turn suggests the necessity for further modifications of the cosmological model: either by dropping the assumption of N_{eff} (or ω_b) being constant, or, as seen above, by admitting a nonzero neutrino chemical potential.

Aside of the massive sterile neutrino scenario, the combination of CMB+LSS and BBN data can of course also be used to constrain the commonly considered case of N_{eff} massless degrees of freedom. We find $N_{\text{eff}} = 3.90^{+0.39}_{-0.56}$ at 95% credibility, with the standard model expectation of $N_{\text{eff}} = 3.046$ outside the 99.5%-credible region, similar to the limits reported in the recent work of Hou *et al.* [9].

4 Conclusions

In this work we have investigated the effects of eV-mass sterile neutrinos, as suggested by global interpretations of neutrino oscillation data, on cosmology. Such sterile neutrinos can thermalise prior to neutrino decoupling, thus contributing to the relativistic energy density in the early universe. However, while the combination of CMB+LSS and BBN data does appear to prefer extra relativistic degrees of freedom at 99.5% credibility within the ΛCDM framework, fully thermalised massive sterile neutrinos in the 1–2 eV mass range necessarily violates the hot dark matter limit on the maximum neutrino mass. In terms of the goodness-of-fit, adding one massless sterile neutrino species improves the CMB+LSS fit by $\Delta\chi_{\text{eff}}^2 = -3.16$ relative to standard ΛCDM , whereas endowing this sterile state with a mass of 1 eV worsens the fit by $\Delta\chi_{\text{eff}}^2 = 4.20$ relative to the same benchmark. Such a scenario is then excluded or strongly disfavoured.

Nonetheless, while it appears difficult to accommodate eV-mass sterile neutrinos within the ΛCDM framework, extending the framework with modifications in the neutrino sector improves to some extent the consistency of sterile neutrinos with precision cosmological data. The simplest such modification is to admit even more additional (effectively massless) relativistic degrees of freedom, not necessarily fully thermalised. Such a scenario improves somewhat the bad effect of the 1 eV sterile neutrino mass at the expense of introducing an additional 1.5 massless species, but the χ_{eff}^2 of the fit is still worse than standard ΛCDM by 2.26 units. Allowing in addition for a dark energy equation of state $w \neq -1$ further improves the fit: for a 1 eV sterile neutrino, a model with $w = -1.11$ and 1.23 additional massless species in fact fits the data marginally better than standard ΛCDM ($\Delta\chi_{\text{eff}}^2 = -0.78$).

Importantly, any model containing eV-mass sterile neutrinos will induce an upward shift in the cold dark matter density inferred from precision cosmological data. This shift can have important consequence for, e.g., the SUSY dark matter parameter space.

However, as is well known, increasing the radiation content in the early universe can be problematic for BBN. We find that while standard BBN prefers roughly an extra relativistic degree of freedom, which we interpret here as a thermalised 1–2 eV sterile neutrino species, additional fully thermalised massless species are strongly disfavoured. Nevertheless, it is

possible to circumvent these BBN constraints with the introduction of a ν_e chemical potential, which itself could have been created by active-sterile oscillations in the early universe. Thus, the state of affairs can be summarised as follows. We need additional radiation to reduce the bad effect of hot dark matter on precision cosmology, and a small neutrino chemical potential to undo the bad effect of too much radiation on BBN. In principle, both of these ingredients can originate from the neutrino sector alone.

In summary, it is not trivial to accommodate a strongly mixed eV-mass sterile neutrino in cosmology. Additional ingredients are required, such as additional radiation, a neutrino chemical potential, or a nontrivial w parameter. In all cases, significant changes in the inferred values of other *a priori* unrelated cosmological parameters are also incurred, e.g., an increase in the cold dark matter density. Thus, should the experimental indications for eV-mass sterile neutrinos become stronger, one must consider a fairly complex modification of the standard Λ CDM cosmology. On the observational side, the upcoming precision measurement of ΔN_{ml} by Planck [46, 47] remains one of the most promising windows to physics beyond the standard model.

Acknowledgements

We acknowledge computing resources from the Danish Center for Scientific Computing (DCSC). JH acknowledges support from a Feodor Lynen-fellowship of the Alexander von Humboldt Foundation. GR acknowledges partial support by the Deutsche Forschungsgemeinschaft under grants No. TR 27 and EXC 153.

References

- [1] J. Kopp, M. Maltoni and T. Schwetz, arXiv:1103.4570.
- [2] E. Akhmedov, T. Schwetz, JHEP **1010** (2010) 115. [arXiv:1007.4171 [hep-ph]].
- [3] S. K. Agarwalla, P. Huber, Phys. Lett. **B696** (2011) 359. [arXiv:1007.3228 [hep-ph]].
- [4] C. Giunti, M. Laveder, [arXiv:1107.1452 [hep-ph]].
- [5] A. D. Dolgov, Phys. Rept. **370** (2002) 333 [hep-ph/0202122].
- [6] Y. I. Izotov, T. X. Thuan, Astrophys. J. **710** (2010) L67.
- [7] J. Hamann, S. Hannestad, G. G. Raffelt, I. Tamborra and Y. Y. Y. Wong, Phys. Rev. Lett. **105** (2010) 181301 [arXiv:1006.5276].
- [8] E. Giusarma, M. Corsi, M. Archidiacono, R. de Putter, A. Melchiorri, O. Mena and S. Pandolfi, Phys. Rev. **D83** (2011) 115023 [arXiv:1102.4774].
- [9] Z. Hou, R. Keisler, L. Knox, M. Millea and C. Reichardt, arXiv:1104.2333.
- [10] R. Keisler *et al.*, arXiv:1105.3182.
- [11] A. X. Gonzalez-Morales, R. Poltis, B. D. Sherwin and L. Verde, arXiv:1106.5052.
- [12] J. R. Kristiansen and Ø. Elgarøy, arXiv:1104.0704
- [13] R. Foot, M. J. Thomson, R. R. Volkas, Phys. Rev. **D53** (1996) 5349 [hep-ph/9509327].
- [14] E. Komatsu *et al.* (WMAP Collaboration), Astrophys. J. Suppl. **192** (2011) 18 [arXiv:1001.4538].
- [15] C. L. Reichardt *et al.*, Astrophys. J. **694** (2009) 1200 [arXiv:0801.1491].
- [16] H. C. Chiang *et al.*, Astrophys. J. **711** (2010) 1123 [arXiv:0906.1181].

- [17] M. L. Brown *et al.* (QUaD collaboration), *Astrophys. J.* **705** (2009) 978 [arXiv:0906.1003].
- [18] B. A. Reid *et al.*, *Mon. Not. Roy. Astron. Soc.* **404** (2010) 60 [arXiv:0907.1659].
- [19] R. Amanullah *et al.*, *Astrophys. J.* **716** (2010) 712 [arXiv:1004.1711].
- [20] A. G. Riess *et al.*, *Astrophys. J.* **699** (2009) 539 [arXiv:0905.0695].
- [21] R. Hlozek *et al.*, arXiv:1105.4887.
- [22] A. Lewis and S. Bridle, *Phys. Rev. D* **66** (2002) 103511 [astro-ph/0205436].
- [23] V. F. Shvartsman, *Pisma Zh. Eksp. Teor. Fiz.* **9** (1969) 315.
- [24] G. Steigman, D. N. Schramm and J. E. Gunn, *Phys. Lett.* **B66** (1977) 202.
- [25] V. Simha, G. Steigman, *JCAP* **0806** (2008) 016 [arXiv:0803.3465].
- [26] O. Pisanti, A. Cirillo, S. Esposito, F. Iocco, G. Mangano, G. Miele and P. D. Serpico, *Comput. Phys. Commun.* **178** (2008) 956 [arXiv:0705.0290].
- [27] P. D. Serpico, S. Esposito, F. Iocco, G. Mangano, G. Miele and O. Pisanti, *JCAP* **0412** (2004) 010 [astro-ph/0408076].
- [28] K. Nakamura *et al.* (Particle Data Group), *J. Phys. G* **G37** (2010) 075021.
- [29] A. Serebrov *et al.*, *Phys. Lett.* **B605** (2005) 72 [nucl-ex/0408009].
- [30] A. Pichlmaier, V. Varlamov, K. Schreckenbach and P. Geltenbort, *Phys. Lett.* **B693** (2010) 221.
- [31] A. P. Serebrov and A. K. Fomin, *Phys. Rev. C* **82** (2010) 035501 [arXiv:1005.4312].
- [32] M. Pettini, B. J. Zych, M. T. Murphy, A. Lewis and C. C. Steidel, *Mon. Not. Roy. Astron. Soc.* **391** (2008) 1499 [arXiv:0805.0594].
- [33] E. Aver, K. A. Olive and E. D. Skillman, *JCAP* **1103** (2011) 043 [arXiv:1012.2385].
- [34] G. Mangano and P. D. Serpico, *Phys. Lett. B* **701** (2011) 296 [arXiv:1103.1261].
- [35] R. Salvaterra and A. Ferrara, *Mon. Not. Roy. Astron. Soc.* **340** (2003) L17 [astro-ph/0302285].
- [36] E. Vangioni, J. Silk, K. A. Olive and B. D. Fields, *Mon. Not. Roy. Astron. Soc.* **413** (2011) 2987 [arXiv:1010.5726].
- [37] F. Spite and M. Spite, *Astron. Astrophys.* **115** (1982) 357.
- [38] A. J. Korn *et al.*, *Nature* **442** (2006) 657 [astro-ph/0608201].
- [39] R. H. Cyburt, B. D. Fields and K. A. Olive, *JCAP* **0811** (2008) 012 [arXiv:0808.2818].
- [40] H. S. Kang and G. Steigman, *Nucl. Phys. B* **372** (1992) 494.
- [41] A. D. Dolgov, S. H. Hansen, S. Pastor, S. T. Petcov, G. G. Raffelt and D. V. Semikoz, *Nucl. Phys. B* **632** (2002) 363 [hep-ph/0201287].
- [42] S. Pastor, T. Pinto and G. G. Raffelt, *Phys. Rev. Lett.* **102** (2009) 241302 [arXiv:0808.3137].
- [43] G. Mangano, G. Miele, S. Pastor, O. Pisanti and S. Sarikas, *JCAP* **1103** (2011) 035 [arXiv:1011.0916].
- [44] S. Hannestad, *JCAP* **0305** (2003) 004 [astro-ph/0303076].
- [45] V. Barger, J. P. Kneller, H. S. Lee, D. Marfatia and G. Steigman, *Phys. Lett. B* **566** (2003) 8 [hep-ph/0305075].
- [46] L. Perotto, J. Lesgourgues, S. Hannestad, H. Tu and Y. Y. Y. Wong, *JCAP* **0610** (2006) 013.
- [47] J. Hamann, J. Lesgourgues and G. Mangano, *JCAP* **0803** (2008) 004.